

# TUNTWIN's Workshop

## Session A: Basics in Synchrotron Techniques for Environmental and Food from Basics to Application



Funded by the Horizon 2020 Framework Programme of the European Union under the GA N° 952306





# Session: X-ray imaging techniques session

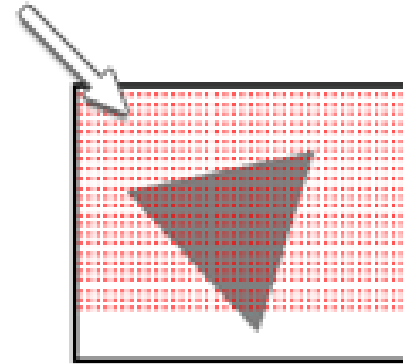
## X-ray microscopy, imaging and tomography

**Roberto Boada**

[roberto.boada@uab.cat](mailto:roberto.boada@uab.cat)

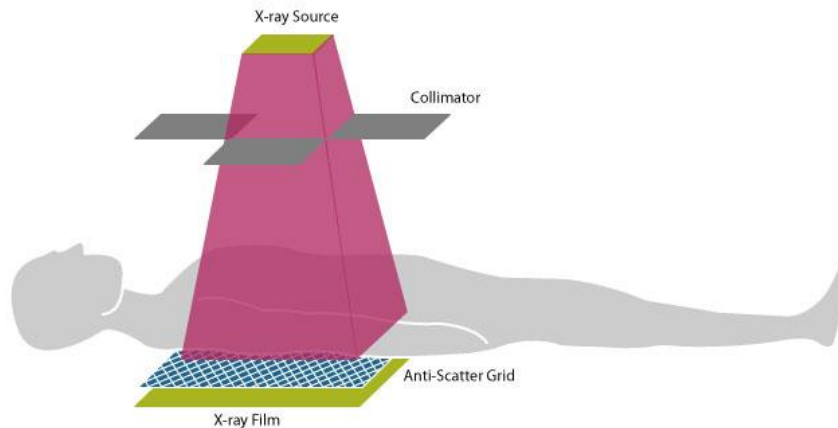
# Spatially resolved information

**Mapping:** using a very small beam ( $\mu\text{m}$  or  $\text{nm}$  size) to raster the sample surface in order to get spatially resolved spectroscopy or diffraction information on every spot.



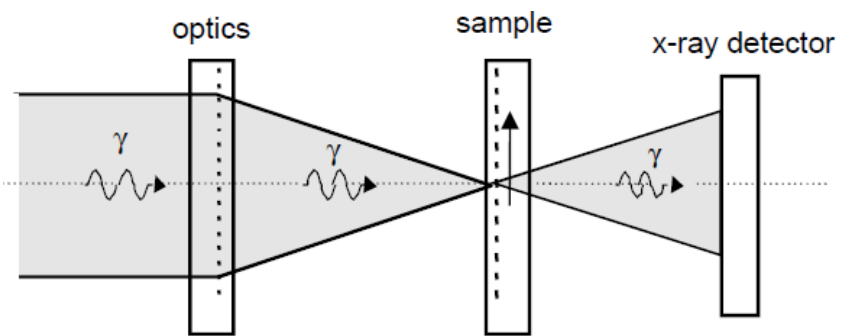
Beam 'rasters' over sample

**Imaging:** use of coherent X-rays to “visualize” the object under study (absorption, phase contrast, diffraction, fluorescence,...).

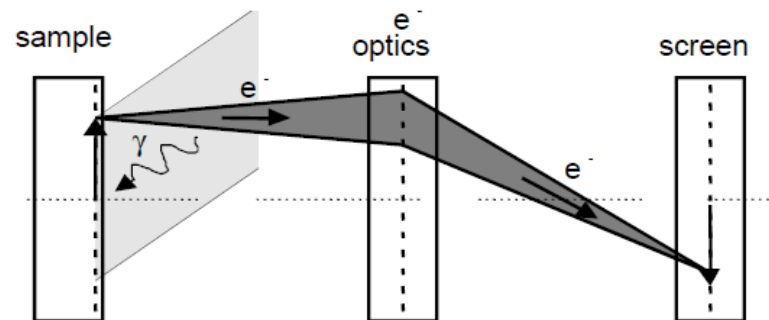
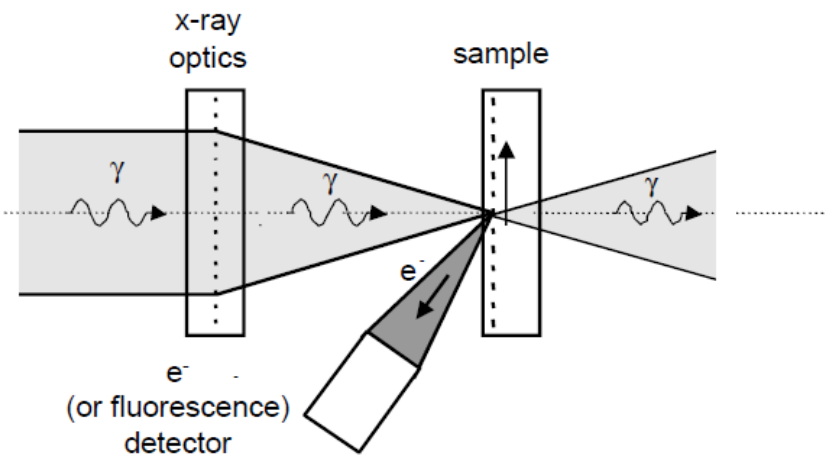
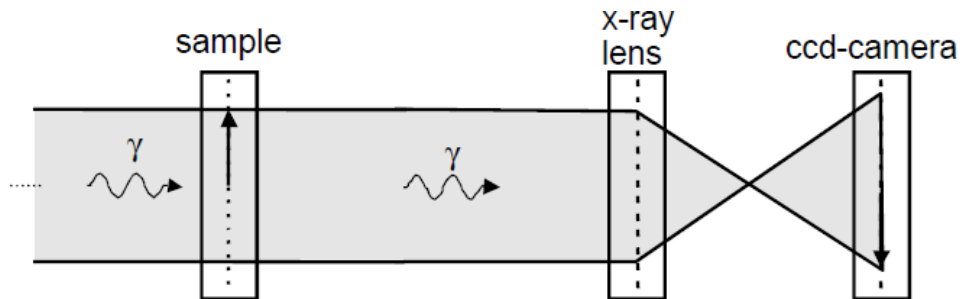


# Spatially resolved information

## $\mu$ -spot illumination

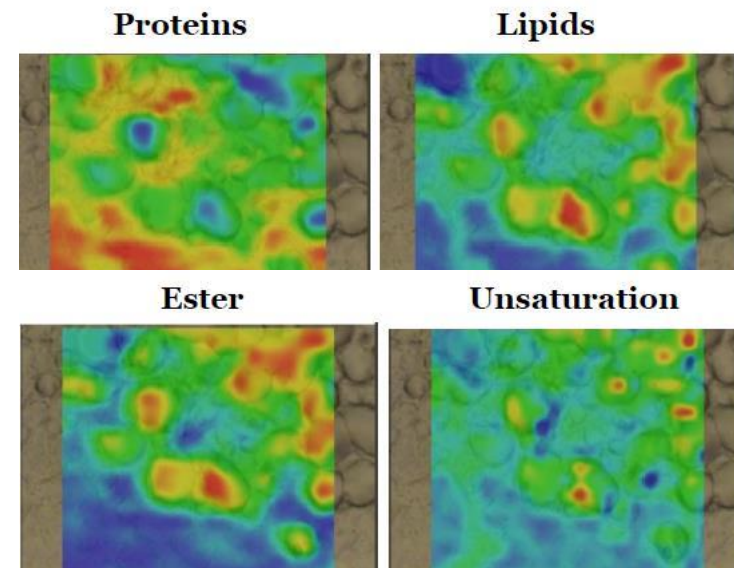
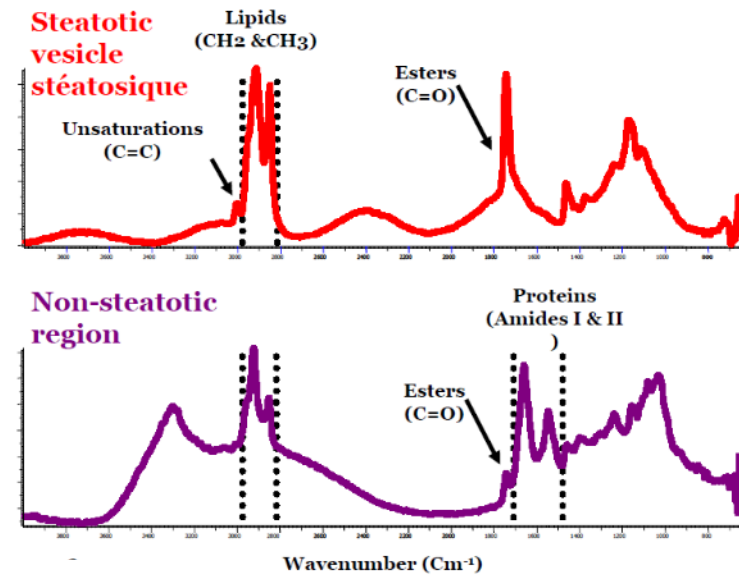
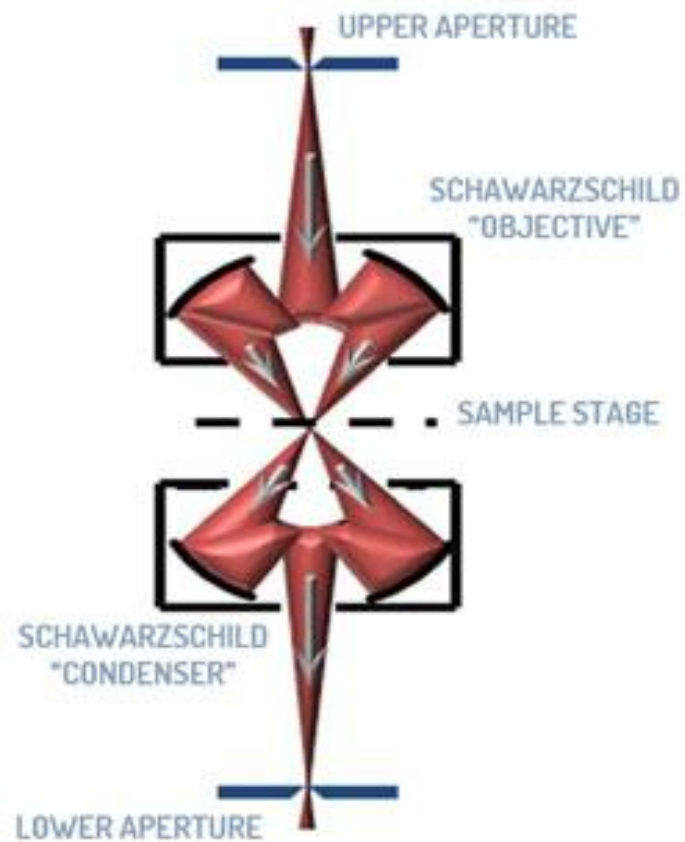


## Homogeneous illumination



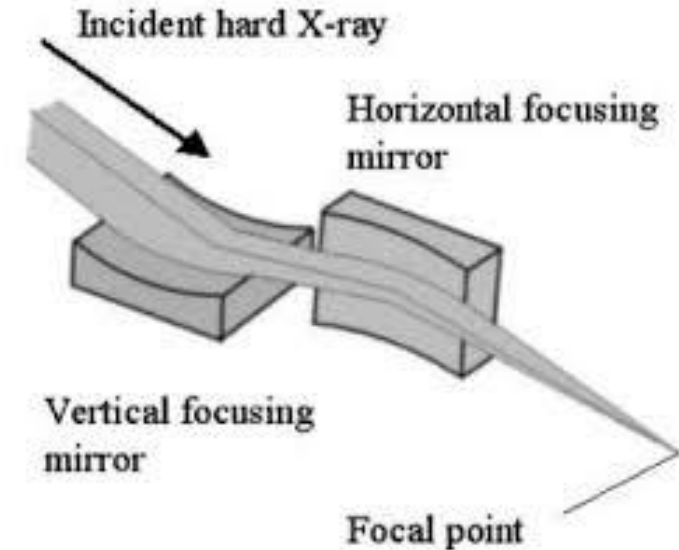
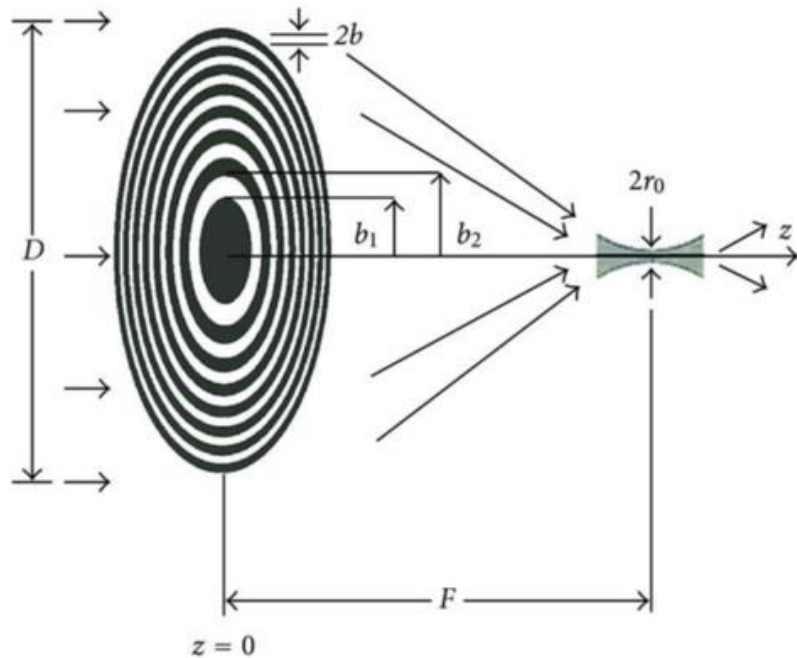
# μFTIR MAPPING

Reflective mirrors (no lenses) in the microscope to reduce the absorption



# MICRO AND NANO FOCUSED BEAMS

**Kirkpatrick-Baez (KB) mirrors** consist of two elliptical mirrors aligned perpendicularly to each other. X-rays from a light source placed at one focus are reflected on the mirror surface and always reach the second focus.

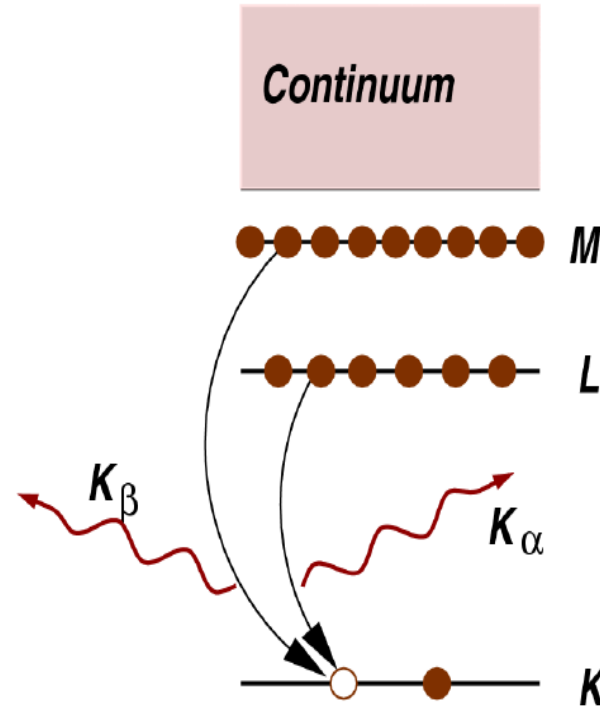


**Fresnel zone plates (diffractive optics)** are comprised of concentric circular zones of two different materials with different absorption or phase shifting properties such that x-rays are diffracted at the interface of the zones onto a focal point.

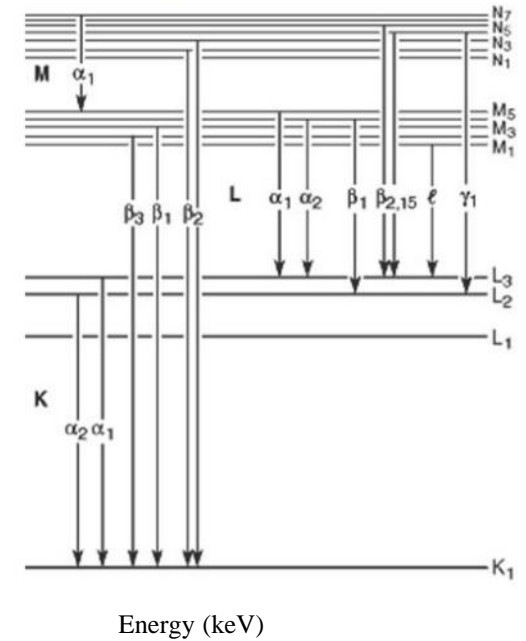
# X-ray fluorescence

After an x-ray absorption, the decay of the excited state: x-ray fluorescence (left) and the Auger effect (right). In both cases, the probability of emission (x-ray or electron) is directly proportional to the absorption probability.

**X-ray fluorescence:** a higher energy electron, core-level electron, fills the deeper core hole, ejecting an x-ray of well-defined energy

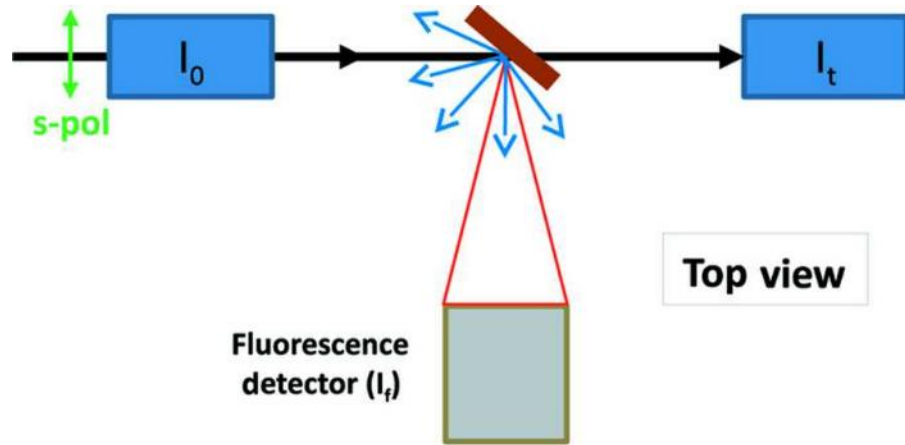


## X-ray emission lines



Element	$K\alpha_1$	$K\alpha_2$
22 Ti	4,510.84	4,504.86
23 V	4,952.20	4,944.64
24 Cr	5,414.72	5,405.509
25 Mn	5,898.75	5,887.65
26 Fe	6,403.84	6,390.84
27 Co	6,930.32	6,915.30
28 Ni	7,478.15	7,460.89
29 Cu	8,047.78	8,027.83
30 Zn	8,638.86	8,615.78
31 Ga	9,251.74	9,224.82
32 Ge	9,886.42	9,855.32
33 As	10,543.72	10,507.99
34 Se	11,222.4	11,181.4

# X-ray fluorescence

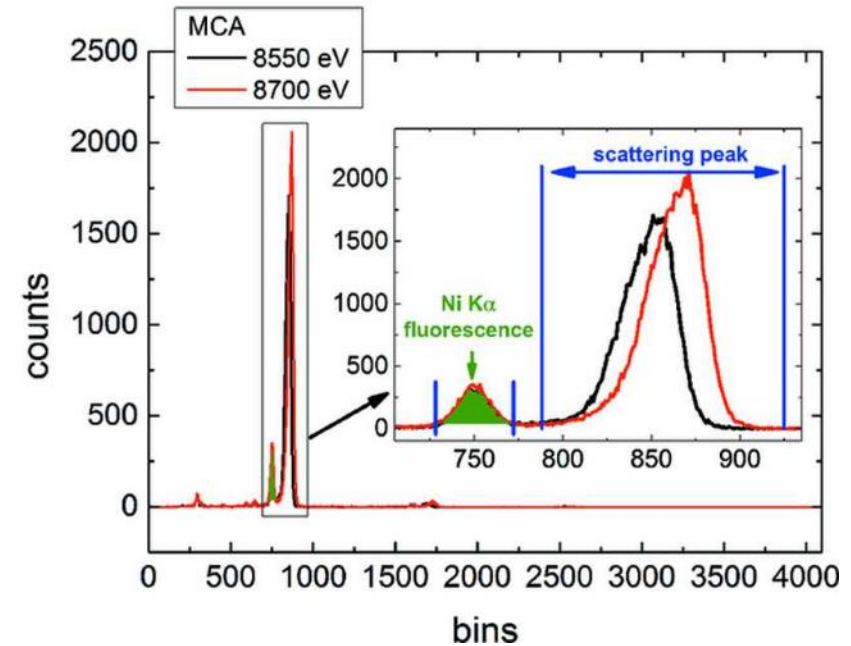


Front view  
(from sample)

56	48	40	32	24	16	8	0
57	49	41	33	25	17	9	1
58	50	42	34	26	18	10	2
59	51	43	35	27	19	11	3
60	52	44	36	28	20	12	4
61	53	45	37	29	21	13	5
62	54	46	38	30	22	14	6
63	55	47	39	31	23	15	7

Approx. X-ray  
beam height

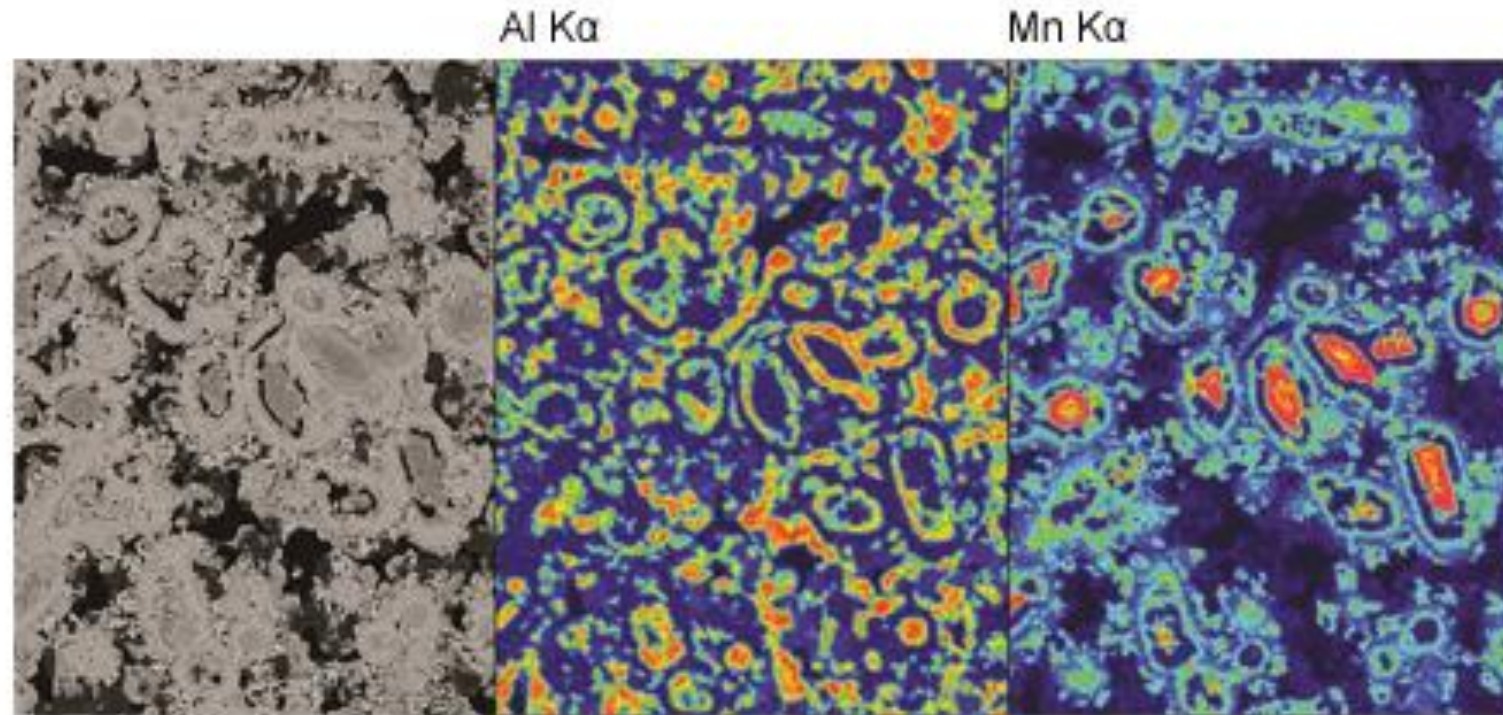
Pulses from  
detector



# X-RAY MAPPING - $\mu$ XRF ( $\mu$ XANES)

X-ray Fluorescence (XRF) mapping provides information about the spatial distribution of elements in a (flat) sample.

- Monitoring the X-ray fluorescence secondary process occurring after the X-ray absorption.
- It is mostly a qualitative technique (concentration determination difficult).

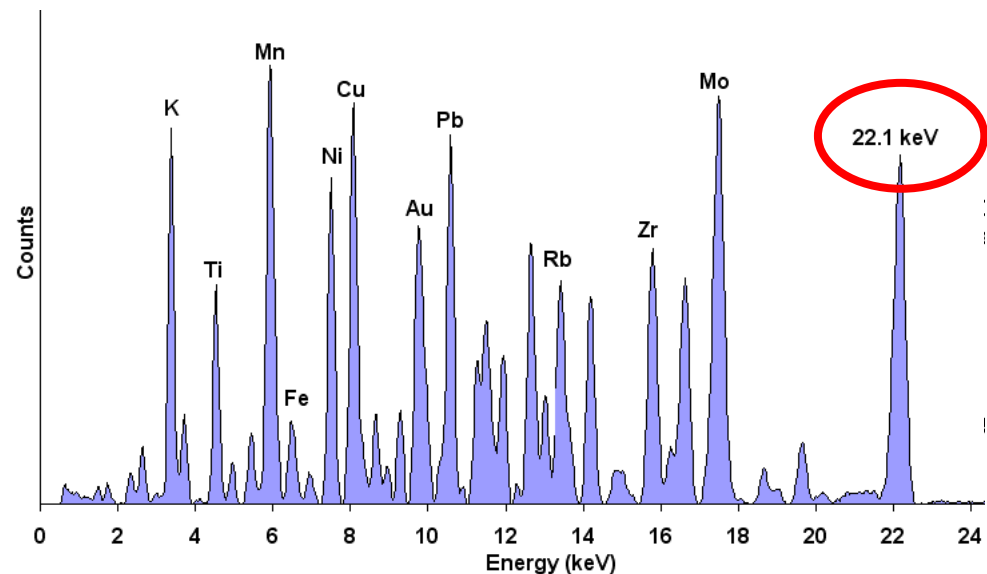


# X-RAY MAPPING - $\mu$ XRF ( $\mu$ XANES)

Energy (keV)		
Element	$K\alpha_1$	$K\alpha_2$
22 Ti	4,510.84	4,504.86
23 V	4,952.20	4,944.64
24 Cr	5,414.72	5,405.509
25 Mn	5,898.75	5,887.65
26 Fe	6,403.84	6,390.84
27 Co	6,930.32	6,915.30
28 Ni	7,478.15	7,460.89
29 Cu	8,047.78	8,027.83
30 Zn	8,638.86	8,615.78
31 Ga	9,251.74	9,224.82
32 Ge	9,886.42	9,855.32
33 As	10,543.72	10,507.99
34 Se	11,222.4	11,181.4
35 Br	11,924.2	11,877.6
36 Kr	12,649	12,598
37 Rb	13,395.3	13,335.8
38 Sr	14,165	14,097.9
39 Y	14,958.4	14,882.9
40 Zr	15,775.1	15,690.9

The acquisition of the the fluorescence (emission) lines characteristic of each element allows to get information about the elemental composition.

These energies are tabulated and allow the correct assignment of the fluorescence peaks measured with an energy dispersive detector which can discriminate the energy of “each” photon detected.



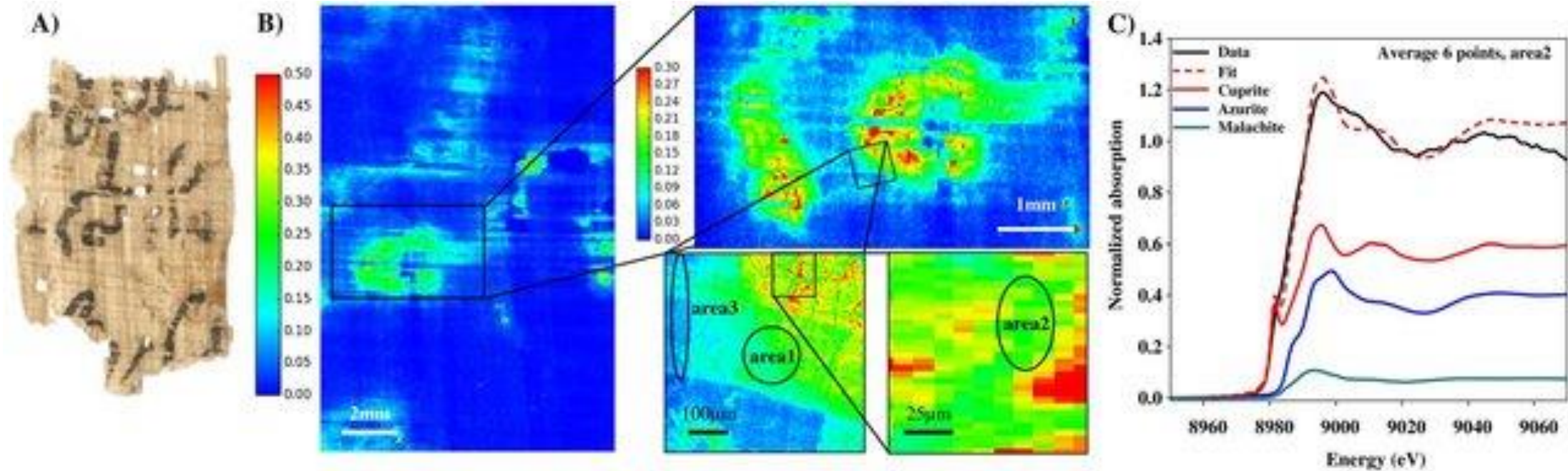
Element	K 1s	L <sub>1</sub> 2s	L <sub>2</sub> 2p <sub>1/2</sub>	L <sub>3</sub> 2p <sub>3/2</sub>
23 V	5465	626.7†	519.8†	512.1†
24 Cr	5989	696.0†	583.8†	574.1†
25 Mn	6539	769.1†	649.9†	638.7†
26 Fe	7112	844.6†	719.9†	706.8†
27 Co	7709	925.1†	793.2†	778.1†
28 Ni	8333	1008.6†	870.0†	852.7†
29 Cu	8979	1096.7†	952.3†	932.7
30 Zn	9659	1196.2*	1044.9*	1021.8*
31 Ga	10367	1299.0*b	1143.2†	1116.4†
32 Ge	11103	1414.6*b	1248.1*b	1217.0*b
33 As	11867	1527.0*b	1359.1*b	1323.6*b
34 Se	12658	1652.0*b	1474.3*b	1433.9*b
35 Br	13474	1782*	1596*	1550*
36 Kr	14326	1921	1730.9*	1678.4*
37 Rb	15200	2065	1864	1804
38 Sr	16105	2216	2007	1940
39 Y	17038	2373	2156	2080
40 Zr	17998	2532	2307	2223
41 Nb	18986	2698	2465	2371
42 Mo	20000	2866	2625	2520

**Incoming intensity must be higher than the absorption edge of the elements of interest**

# X-RAY MAPPING - $\mu$ XRF ( $\mu$ XANES)

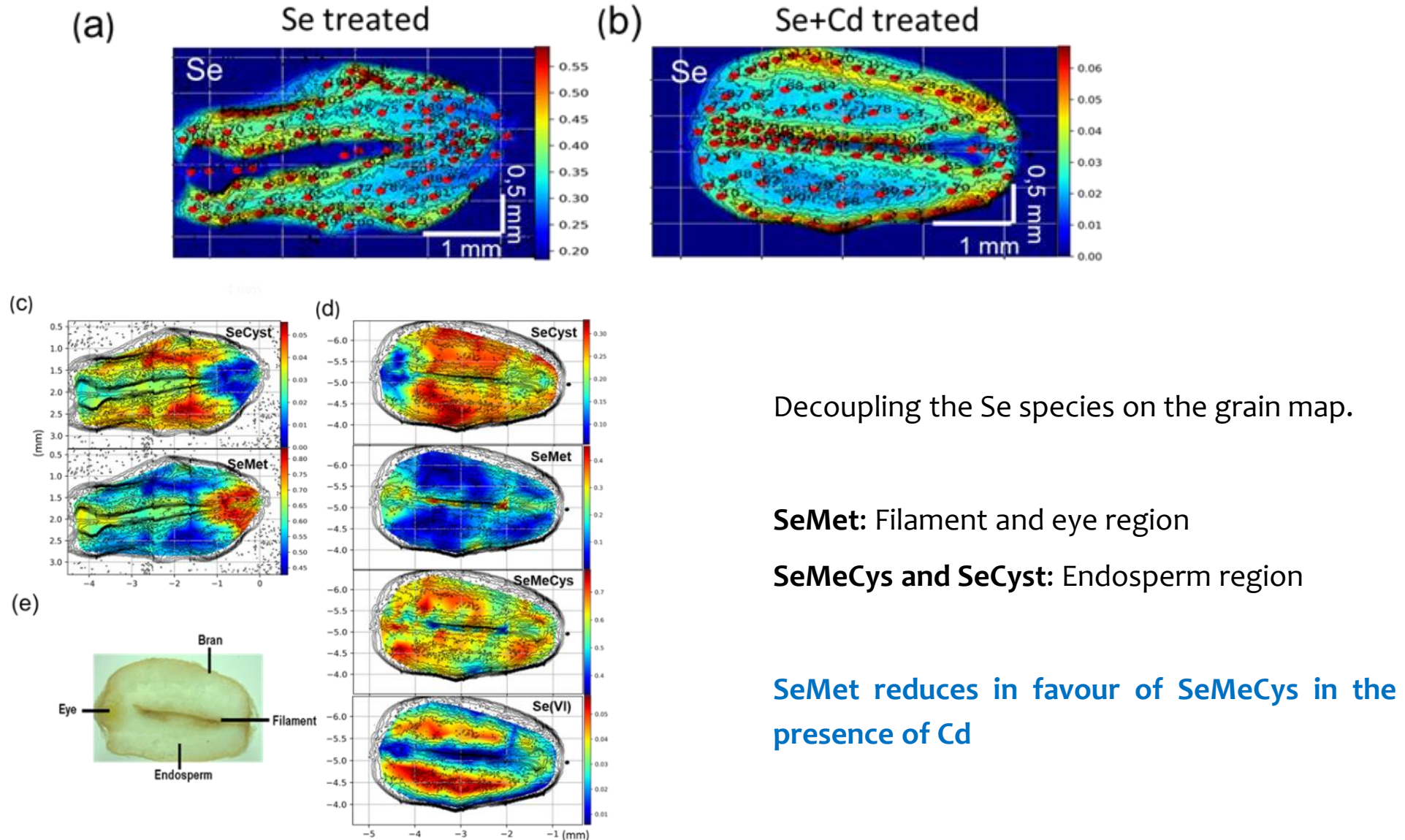
The measurement of X-ray spectrum at representative spots provides chemical information on selected elements.

It is possible to get chemical images...



The nature of ancient Egyptian copper-containing carbon inks is revealed by synchrotron radiation based X-ray microscopy  
Scientific Reports volume 7, Article number: 15346 (2017)

# X-RAY MAPPING - $\mu$ XRF ( $\mu$ XANES)



Decoupling the Se species on the grain map.

**SeMet:** Filament and eye region

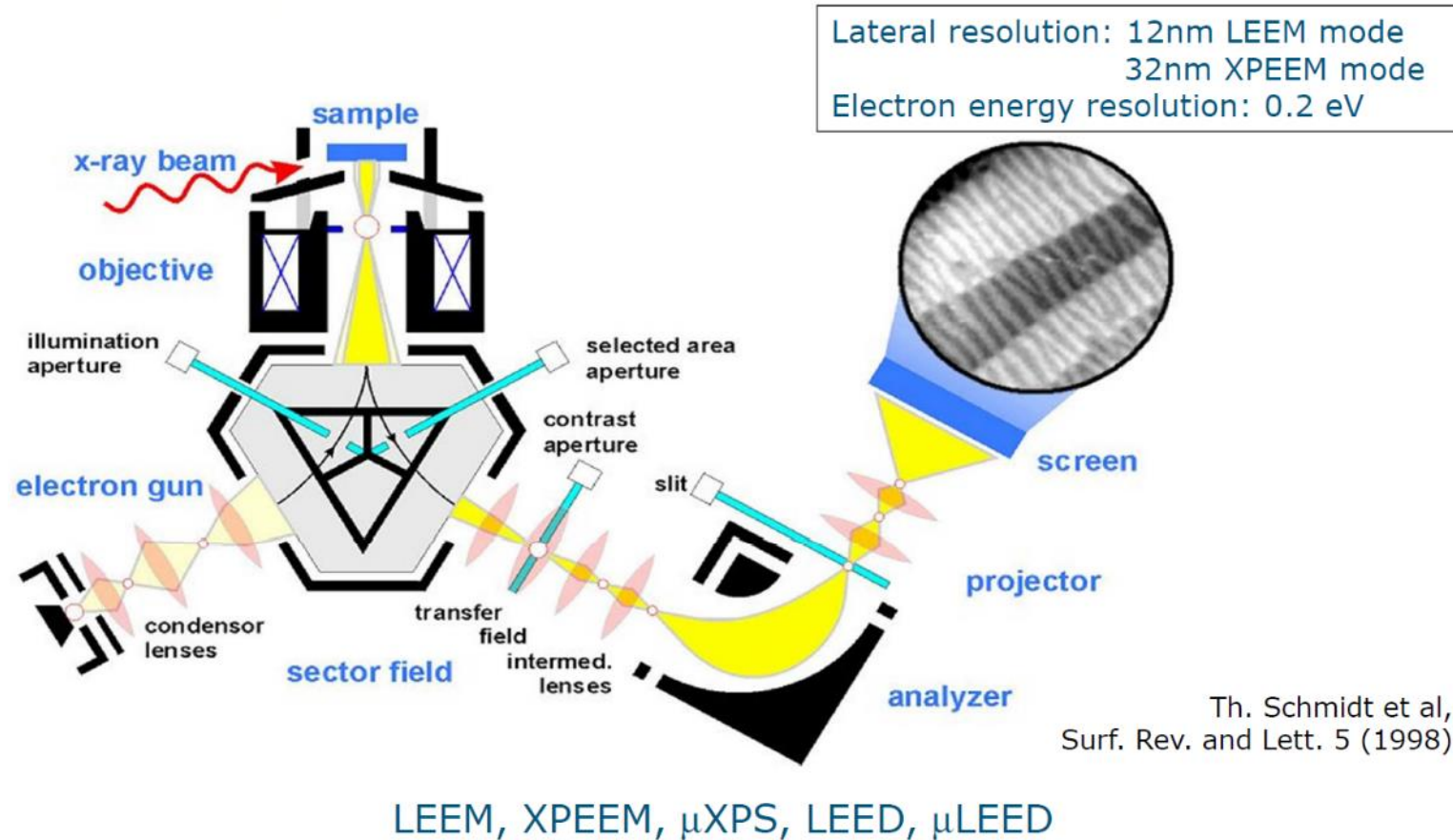
**SeMeCys and SeCyst:** Endosperm region

**SeMet reduces in favour of SeMeCys in the presence of Cd**

# X-RAY MAPPING – Photoemission electron microscopy

**XPEEM:** X-ray Photoemission Electron Microscopy

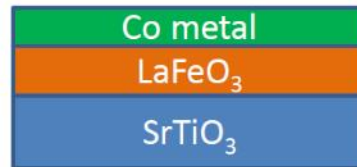
Combining X-ray photoemission spectroscopy with Electron Microscopy



# X-RAY MAPPING – Photoemission electron microscopy

**Samples requirements: flat, conductive, UHV compatible**

**Applications:** Study of magnetic domains in magnetic materials (thin films): AFM and FM

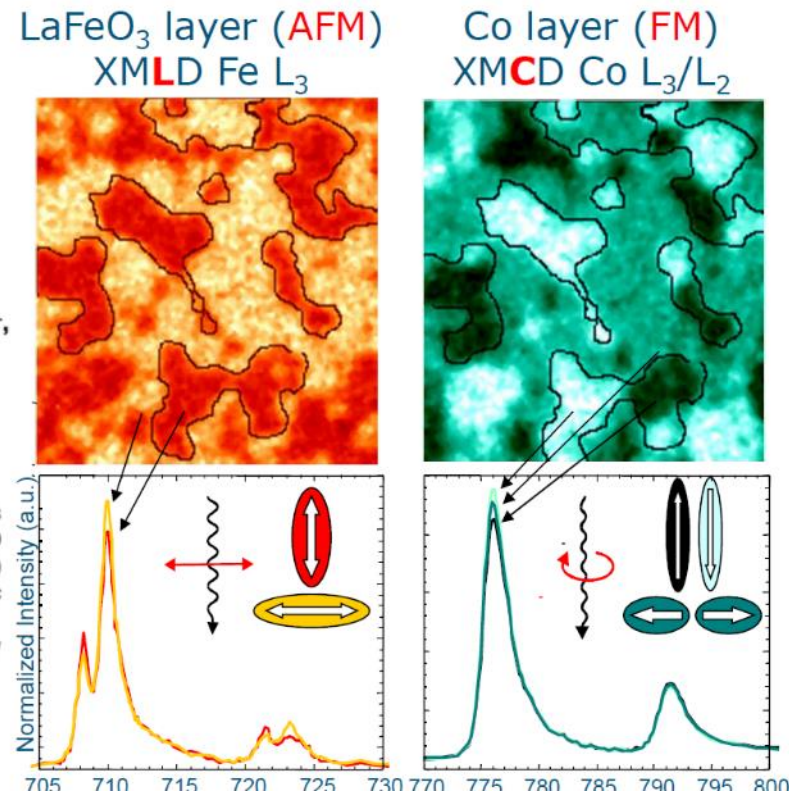


## Direct observation of the alignment of ferromagnetic spins by antiferromagnetic spins

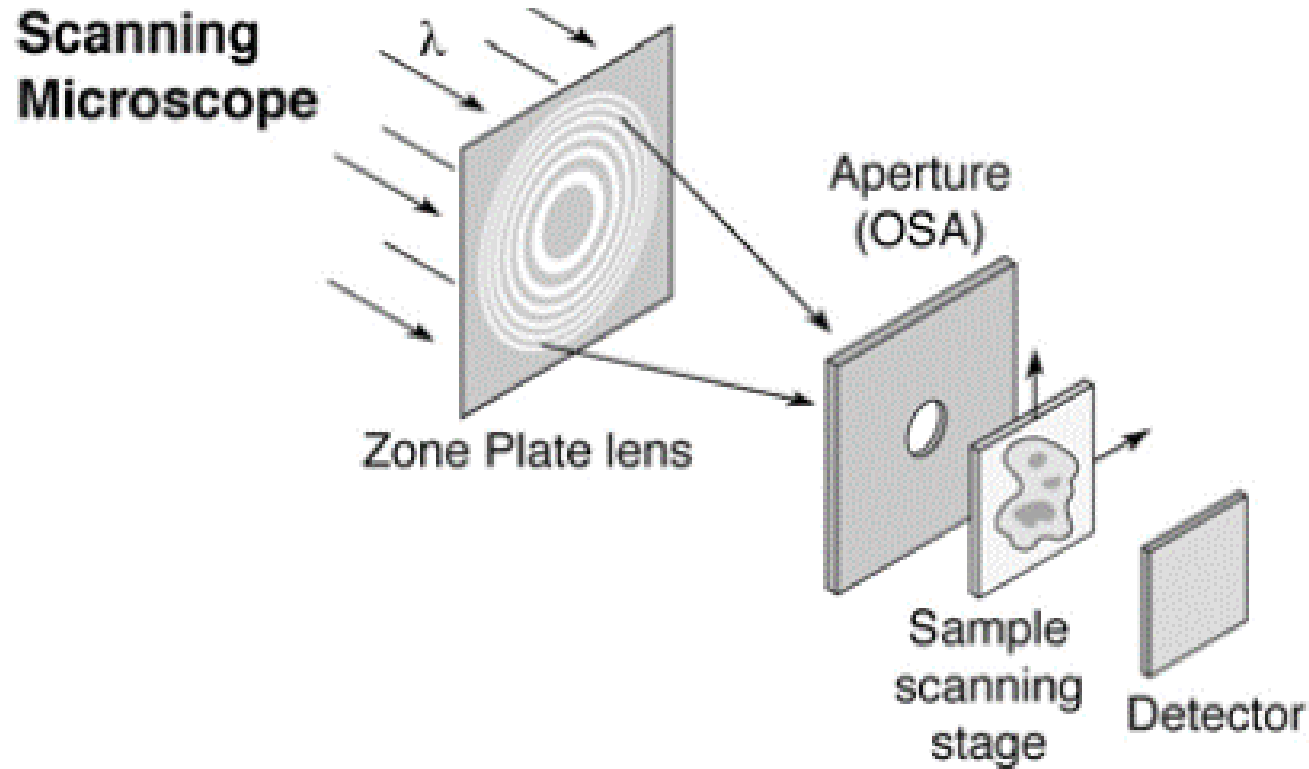
F. Nolting<sup>\*</sup>, A. Scholl<sup>\*</sup>, J. Stöhr<sup>†</sup>, J. W. Seo<sup>‡§</sup>, J. Fompeyrine<sup>§</sup>, H. Siegwart<sup>§</sup>, J.-P. Locquet<sup>§</sup>, S. Anders<sup>\*</sup>, J. Lüning<sup>†</sup>, E. E. Fullerton<sup>†</sup>, M. F. Toney<sup>†</sup>, M. R. Scheinfein<sup>||</sup> & H. A. Padmore<sup>\*</sup>

Nature, 405 (2000), 767.

**Figure 1** Images and local spectra from the antiferromagnetic and ferromagnetic layers for 1.2-nm Co on LaFeO<sub>3</sub>/SrTiO<sub>3</sub>(001). **a**, Fe L-edge XMLD image; **b**, Co L-edge XMCD image. The contrast in the images arises from antiferromagnetic domains in LaFeO<sub>3</sub> (**a**) and ferromagnetic domains in Co (**b**) with in-plane orientations of the antiferromagnetic axis and ferromagnetic spins as indicated below the images. The spectra shown underneath were recorded in the indicated areas and illustrate the origin of the intensity contrast in the PEEM images.



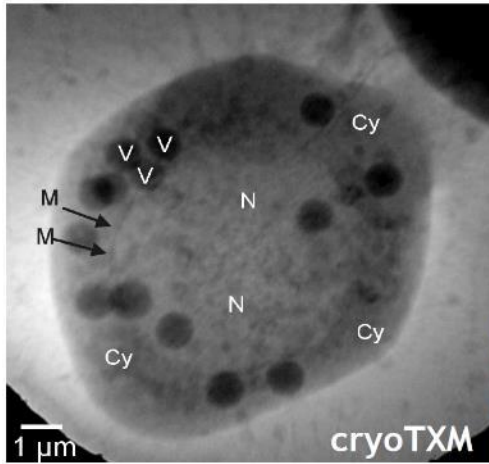
# Scanning transmission X-ray microscopy (STXM)



- 10–20 nm spatial resolution
- Least radiation dose
- Best spectral resolution
- Requires spatially coherent radiation
- Minutes exposure time
- Flexible sample environment
- Photoemission, fluorescence imaging

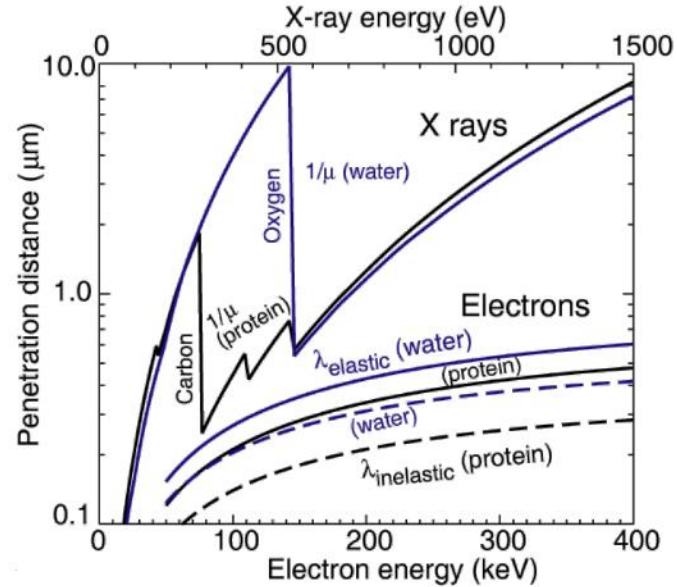
# Scanning transmission X-ray microscopy (STXM)

## Drosophila melanogaster cell

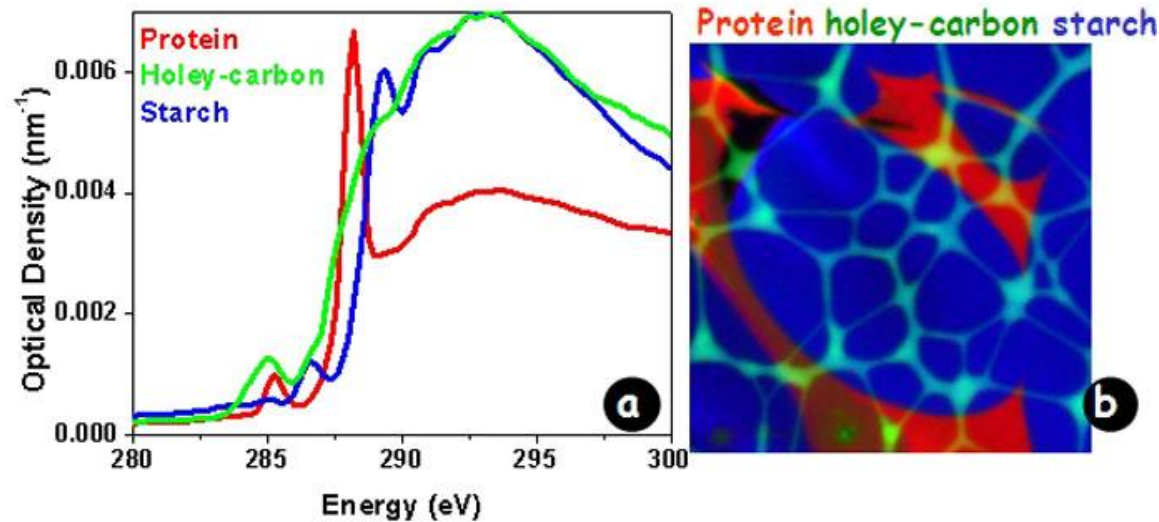


- *Drosophila melanogaster* cell, in vitrified ice, imaged @ 0.5 keV @ BESSY

Cy: cytoplasm  
V: vesicle  
M: nuclear membrane  
N: nucleus

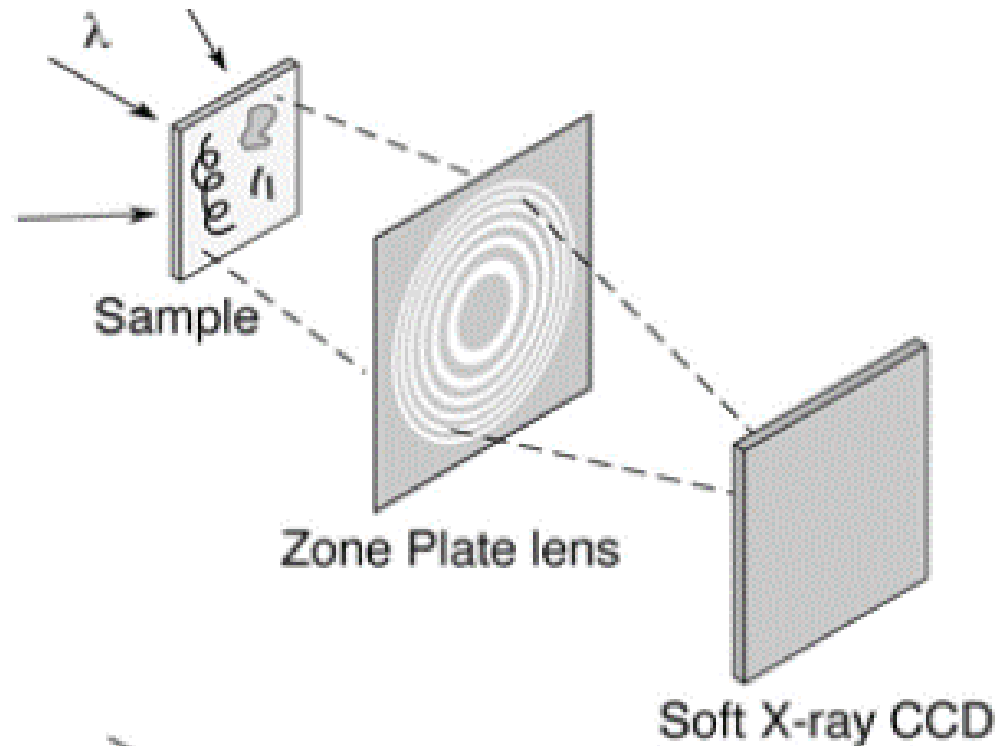


- Natural contrast between protein and water in the so-called **water window**
- Spatial resolution not limited by wavelength



# X-ray fullfield imaging

## Full-Field Microscope



- 10–20 nm spatial resolution
- Modest spectral resolution
- Seconds exposure time
- Bending magnet radiation
- Higher radiation dose
- Flexible sample environment (wet, cryo, labeled magnetic fields, electric fields, cement, ...)

# X-ray imaging – multicontrast imaging

## In-vivo dark-field and phase-contrast x-ray imaging



(a) Conventional x-ray image based on attenuation.

# X-ray imaging – multicontrast imaging

## In-vivo dark-field and phase-contrast x-ray imaging

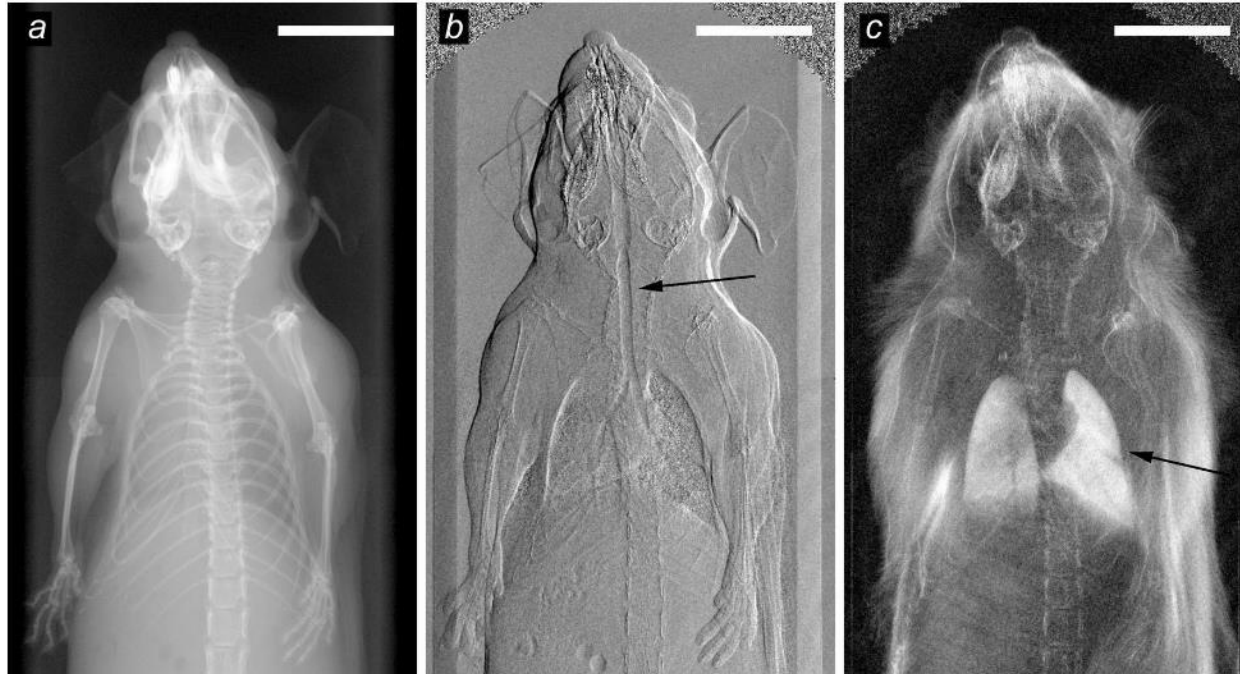


(a) Conventional x-ray image based on attenuation.

(b) Differential phase-contrast image based on x-ray refraction.

# X-ray imaging – multicontrast imaging

## In-vivo dark-field and phase-contrast x-ray imaging



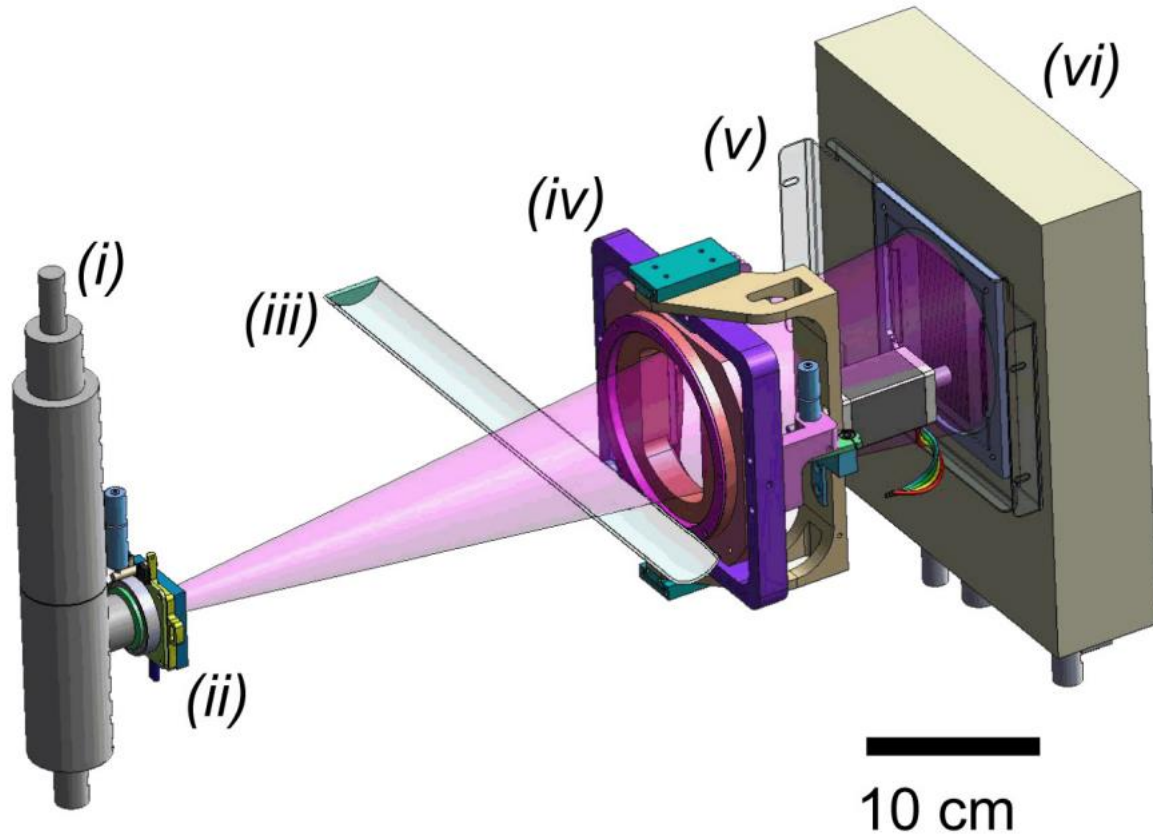
(a) Conventional x-ray image based on attenuation.

(b) Differential phase-contrast image based on x-ray refraction.

(c) Dark-field image based on x-ray scattering.

# X-ray imaging – multicontrast imaging

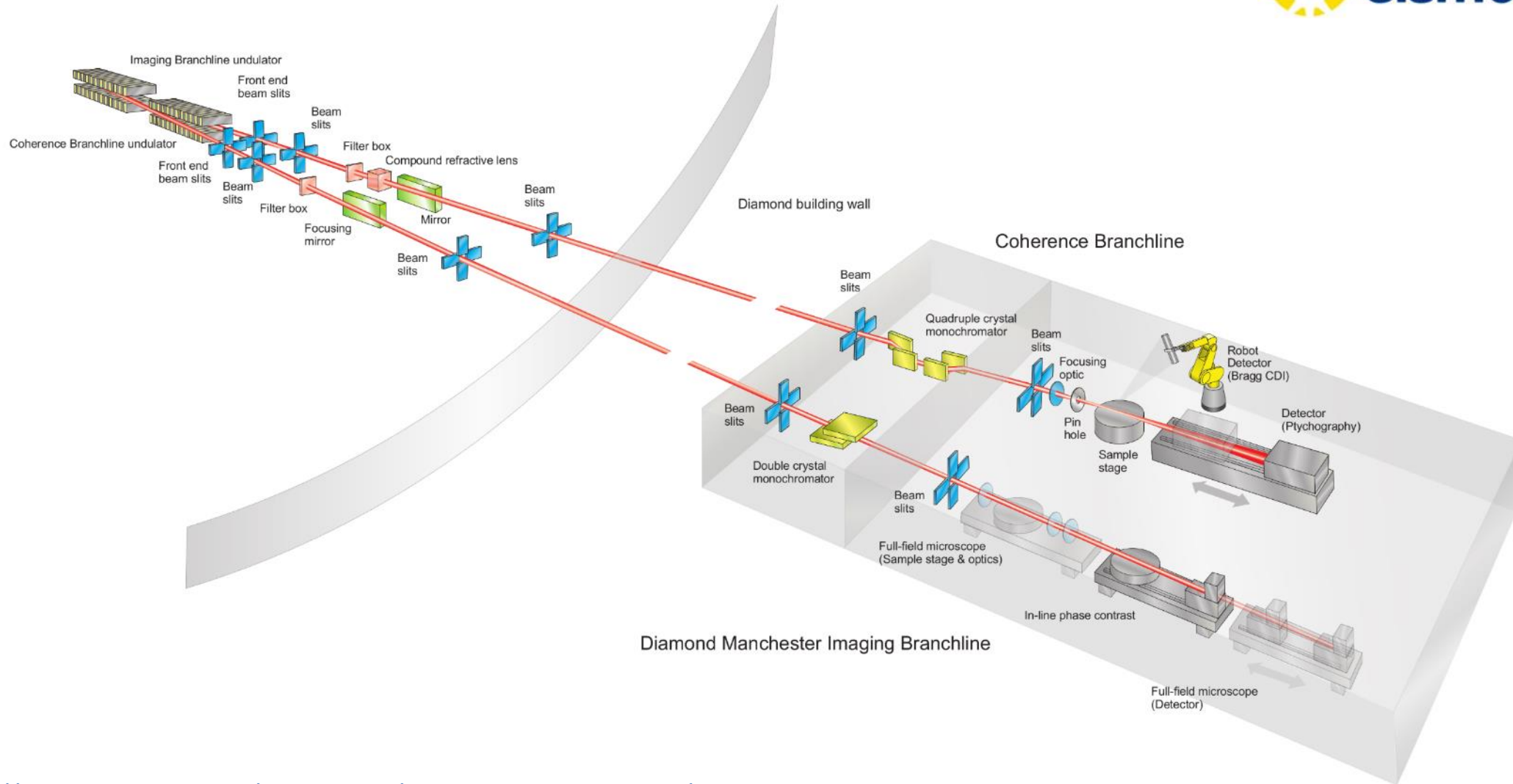
## In-vivo dark-field and phase-contrast x-ray imaging



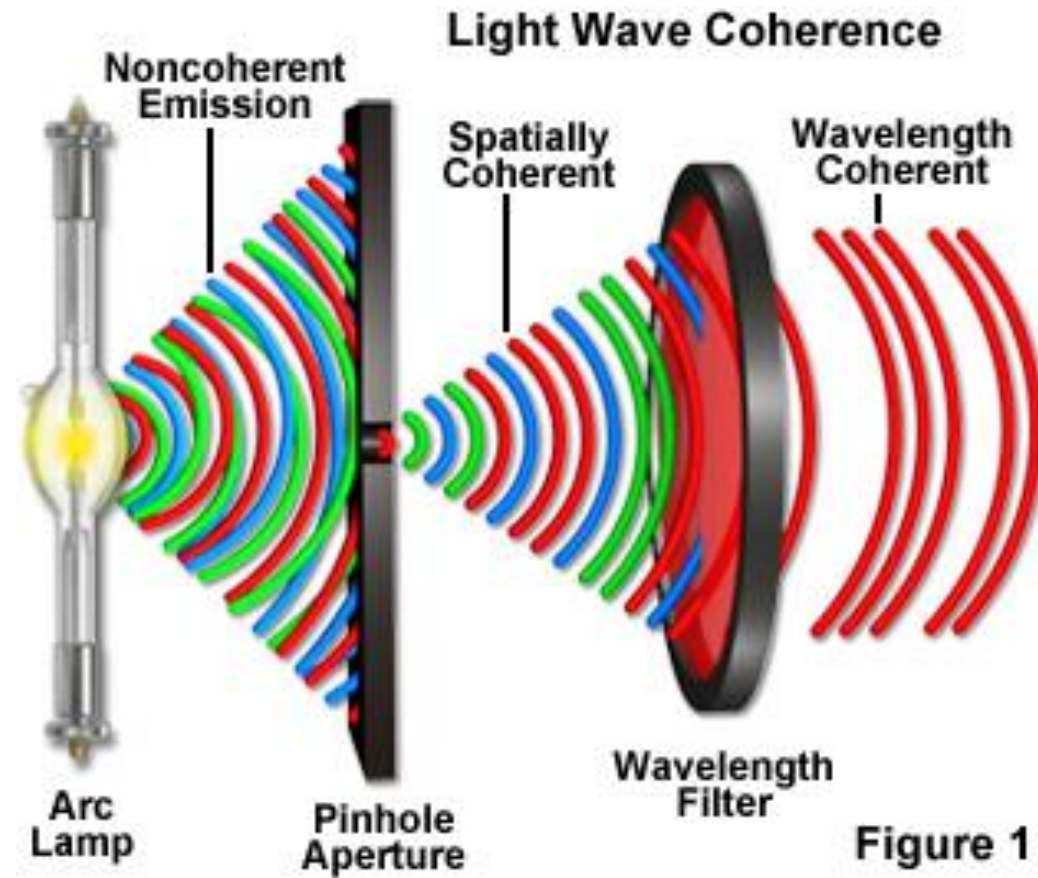
To extract this information, three x-ray transmission gratings are located in the x-ray beam path: one behind the source, one behind the specimen and one right in front of the detector. Together they form an **interferometer**, producing an interference pattern, which is analyzed to retrieve the multi-contrast x-ray image with three different contrast channels.

# X-ray imaging and coherence

## I13: X-ray Imaging and Coherence beamline



# X-ray imaging and coherence



# X-ray imaging and coherence

## I13: X-ray Imaging and Coherence beamline



### Coherence Branchline (I13-1)

Coherent diffraction imaging (CDI) methods. X-rays are diffracted by a sample, and the diffraction patterns are used to reconstruct an image via an iterative feedback algorithm which aims to retrieve the lost phase information.

In effect, the objective lens of a typical microscope is replaced by software.

### Ptychography (Scanning Diffraction Microscopy)

The X-ray beam is focused onto a sample so that a small area is illuminated. The sample is then moved with respect to the beam to create a sequential array of overlapping illuminated areas. For each area, the light scattered by the sample is recorded as a diffraction pattern.

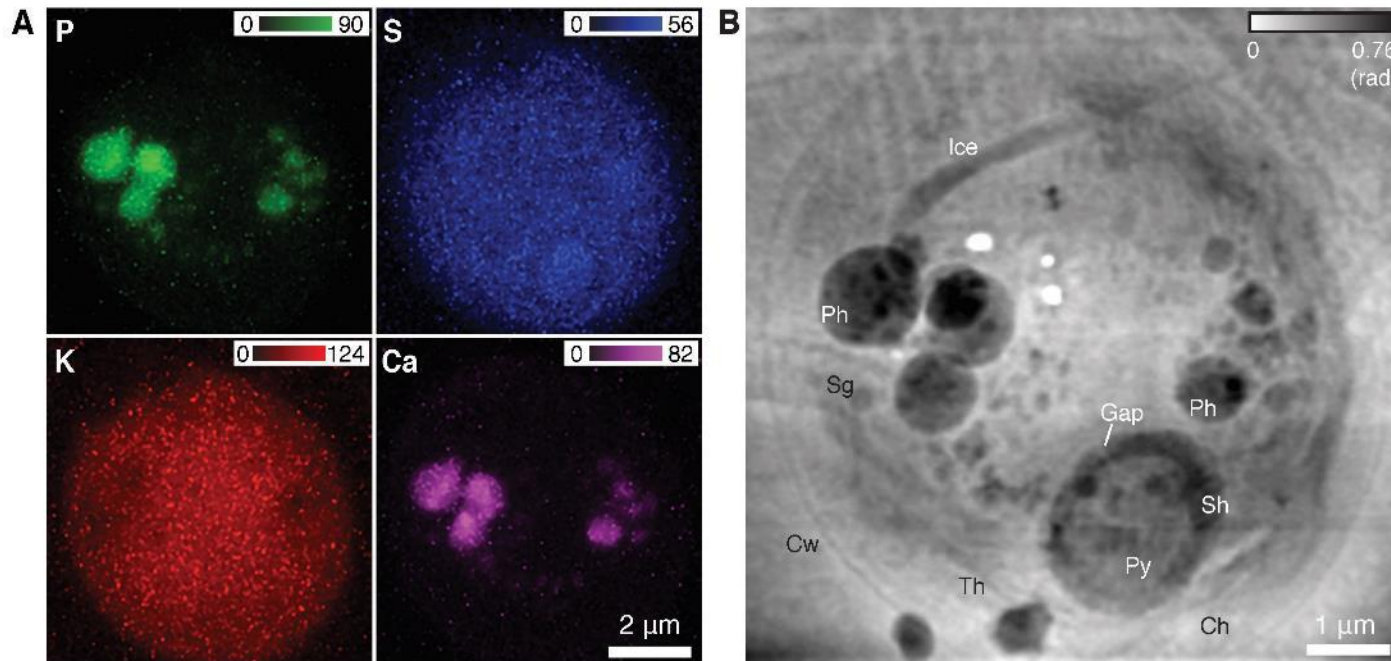
The output is a pair of images. One is a measure of the extent to which light has been absorbed by the sample. The other is a measure of the phase delay introduced to the beam as it passed through the sample. The diffraction patterns are then processed with an iterative algorithm which retrieves the phase information.

# X-ray imaging and coherence

## I13: X-ray Imaging and Coherence beamline



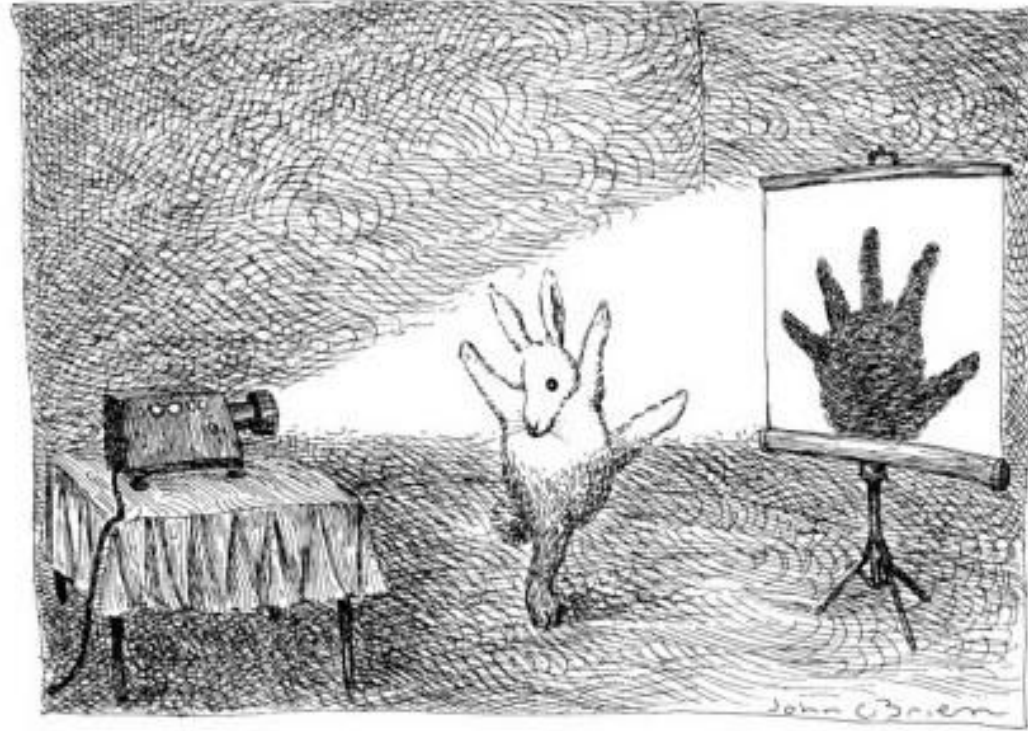
### Ptychography (Scanning Diffraction Microscopy)



### Green algae (*Chlamydomonas reinhardtii*)

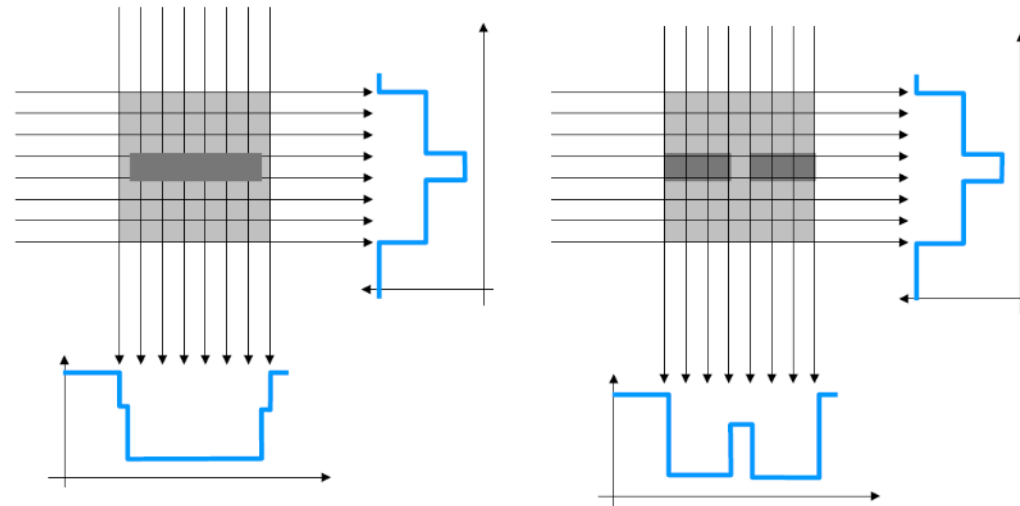
Ptychographs revealed in amazing detail the organelles and membranes which do not fluoresce. Taken together the ptychographs aid identification of the cellular components and the quantified elemental concentrations may reveal the underlying cause of diseases and disorders in studies of cells.

# X-ray tomography



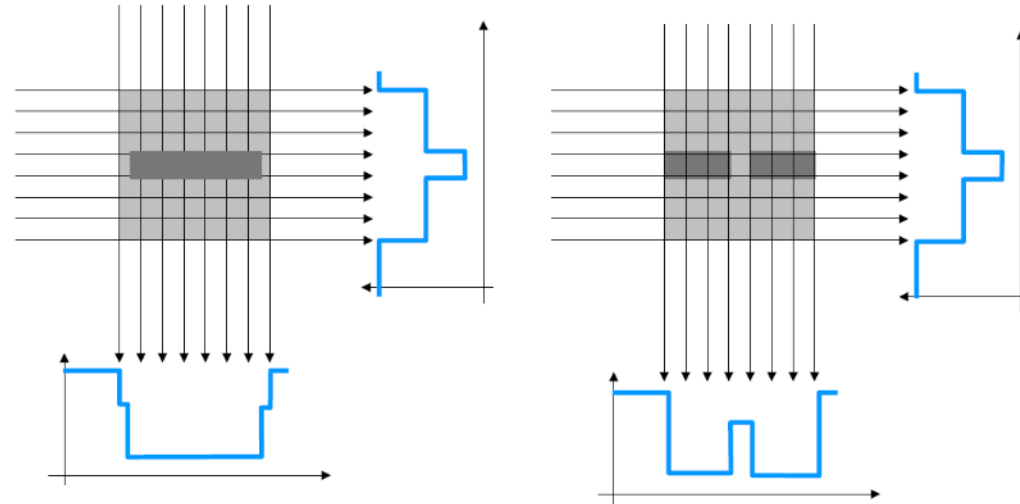
2D approach can be misleading... 3D preferred

# X-ray tomography



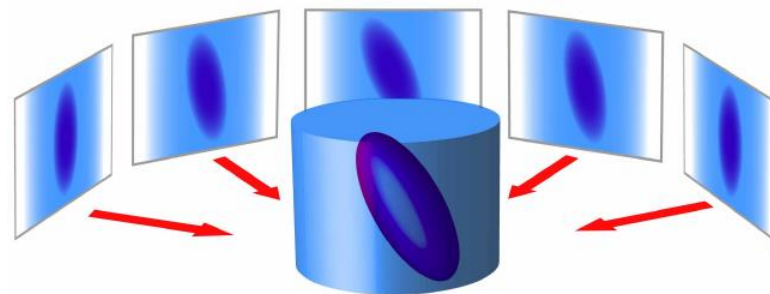
To distinguish the 2 : take at least 2 projections at 90 degrees

# X-ray tomography

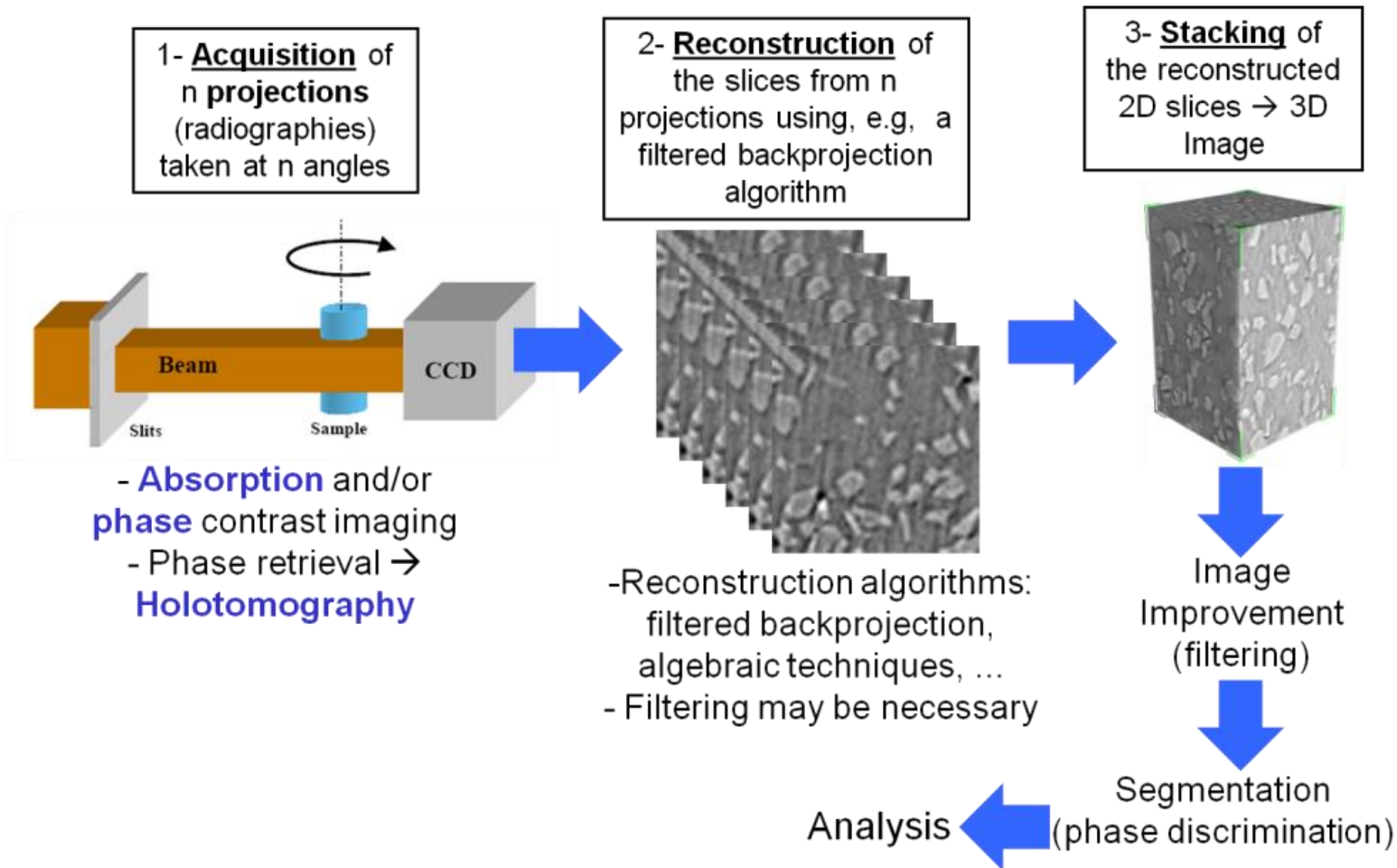


To distinguish the 2 : take at least 2 projections at 90 degrees

In reality, more than 2 projections are needed to reconstruct the 3D object.

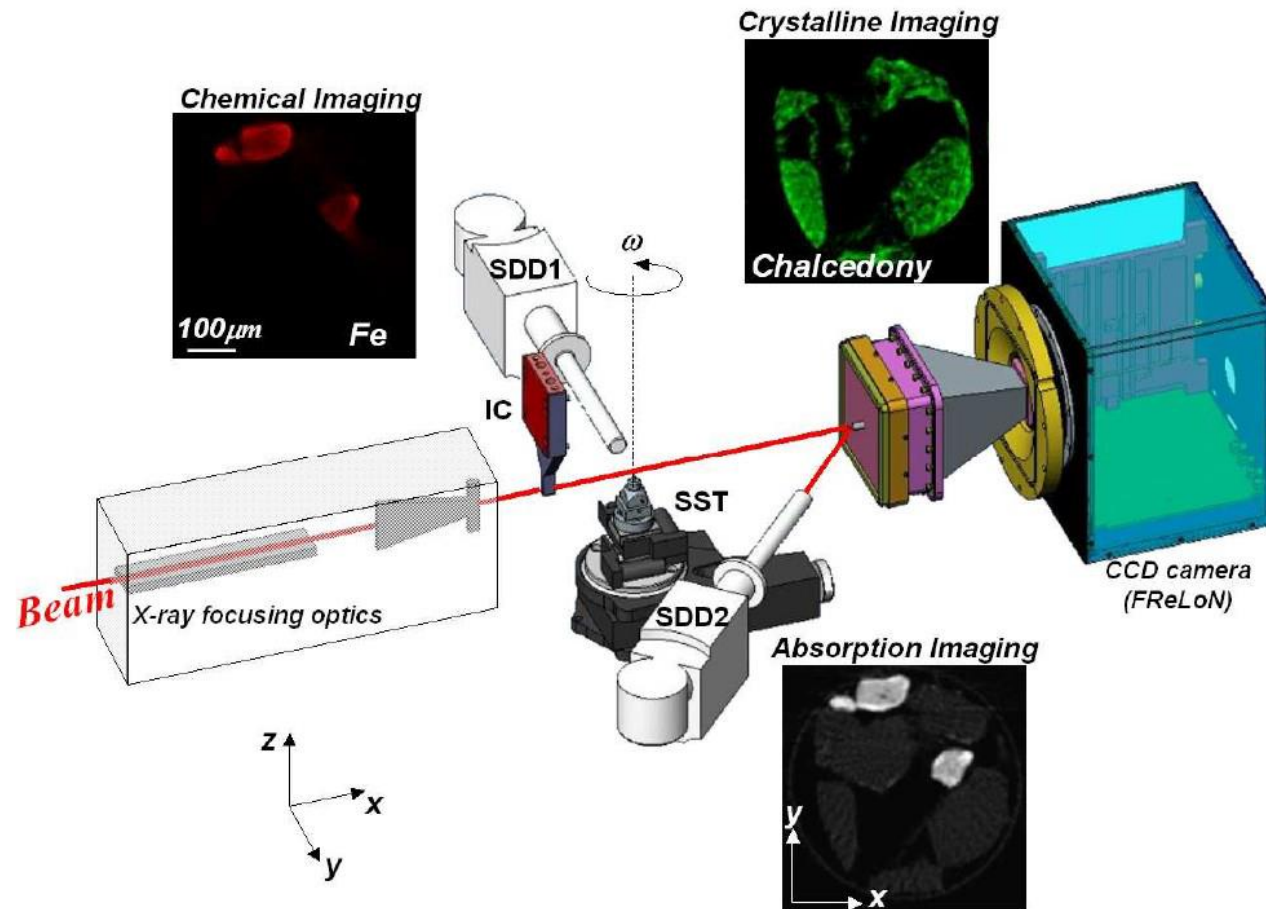


# X-ray tomography



# X-ray tomography

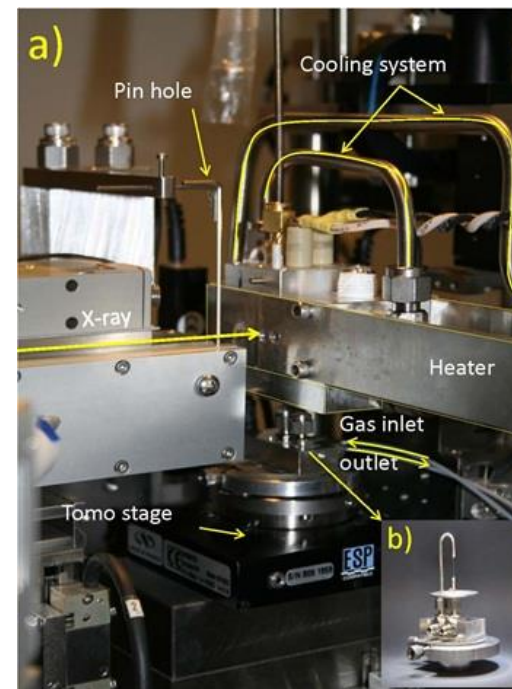
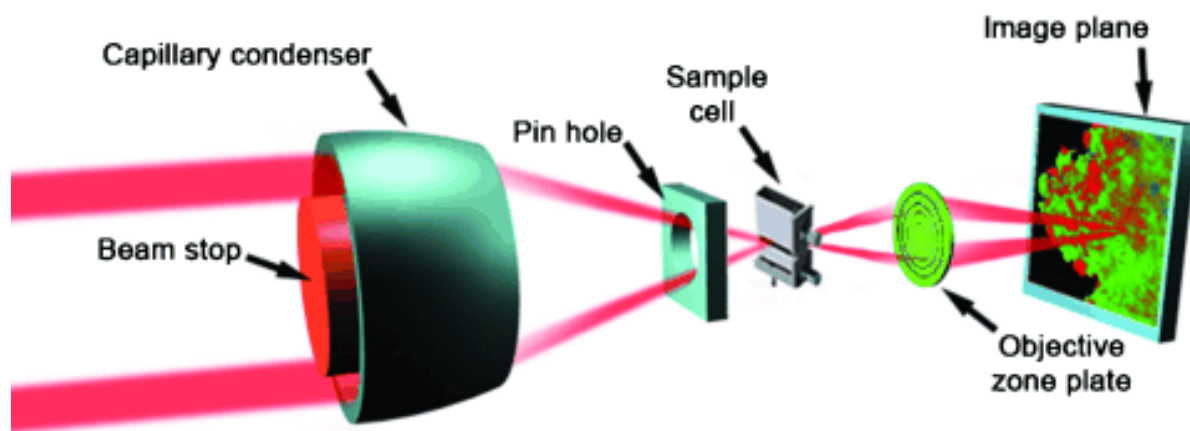
Combining techniques: diffraction-tomography +  $\mu$ XRF + “radiography”



# X-ray tomography

## Hard X-ray Nanotomography using TXM: Fischer-Tropsch Catalyst Nanoscale Chemistry under Realistic Working Conditions

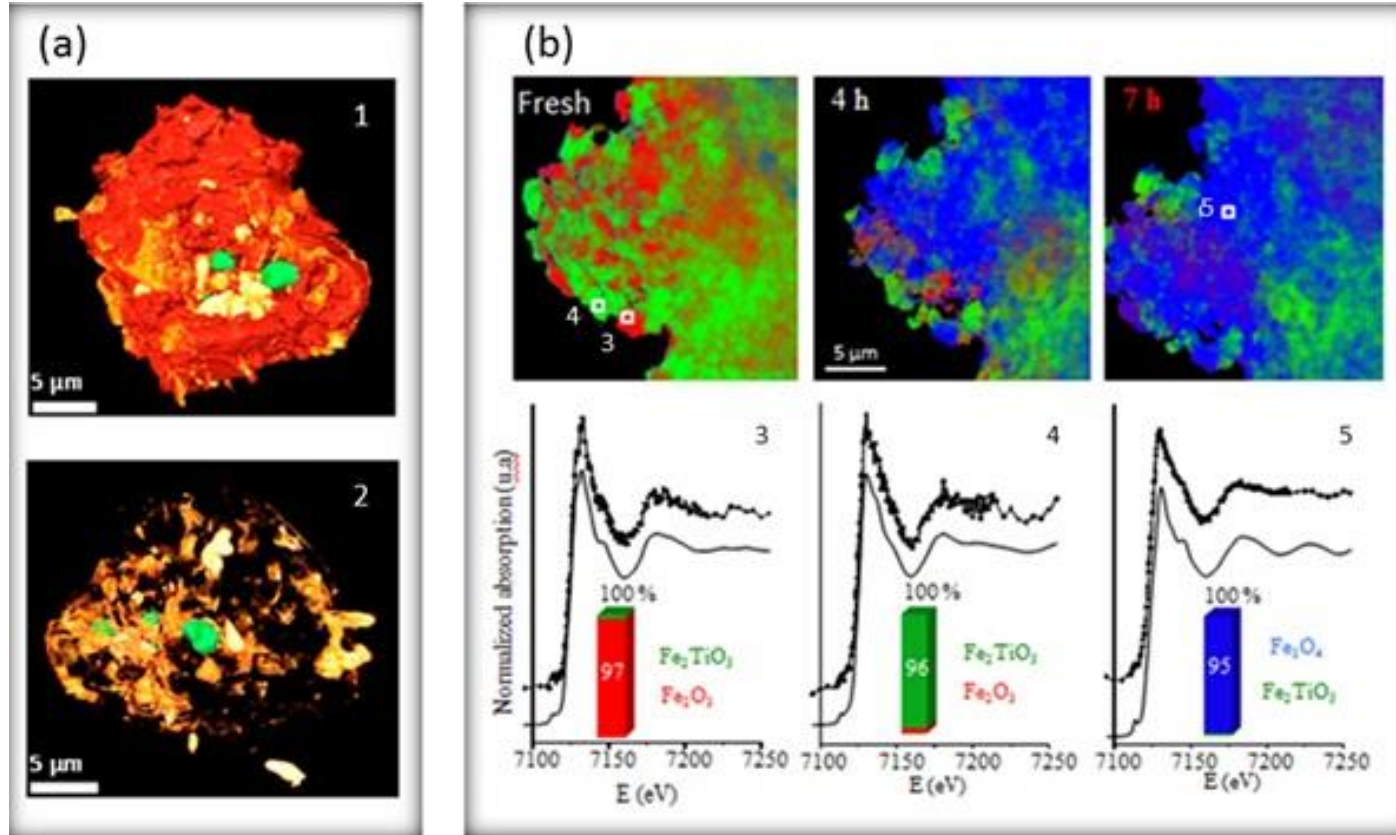
The combination of chemical information with high spatial resolution is even more valuable when the system under study has a marked dynamic character in the catalytically active phases, as is the case for Fe-based catalysts for Fischer-Tropsch-to-Olefins synthesis.



# X-RAY IMAGING – TOMOGRAPHY

Hard X-ray Nanotomography using TXM:

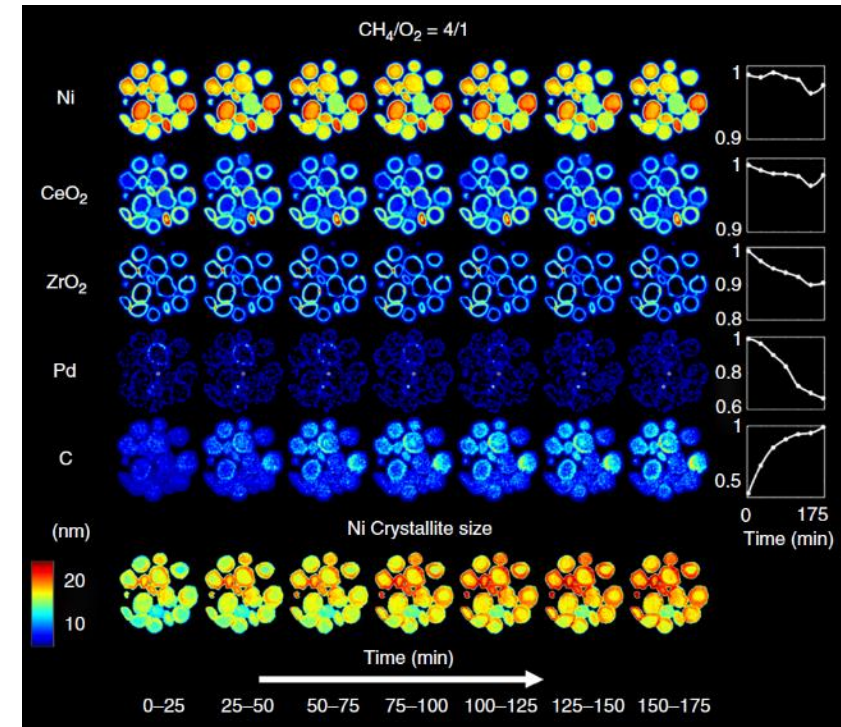
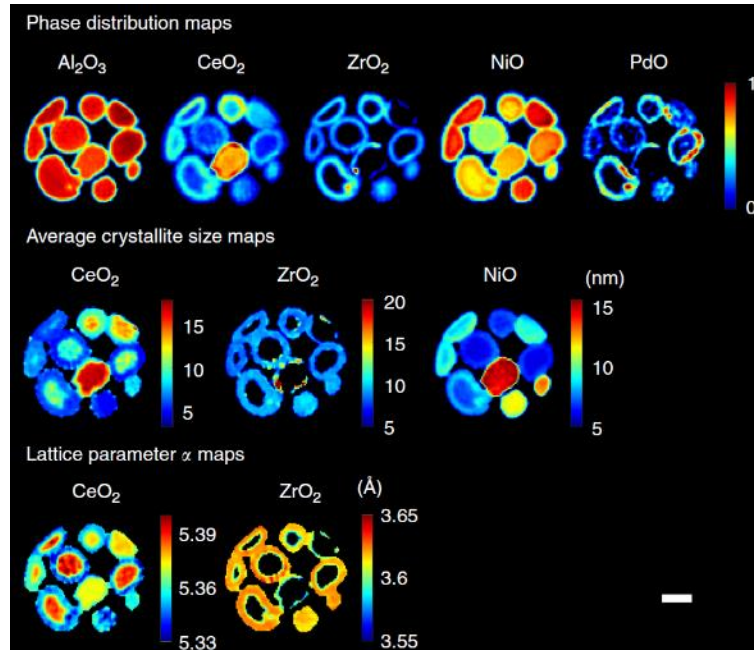
Fischer-Tropsch Catalyst Nanoscale Chemistry under Realistic Working Conditions



By studying the evolution of the species during reaction, it was noted that Fe<sub>2</sub>O<sub>3</sub> was reduced before Fe<sub>2</sub>TiO<sub>5</sub>, which was still present after 5 hours of reaction. After 7 hours of reaction, the iron phase was fully reduced to catalytically active species: Fe<sub>3</sub>O<sub>4</sub> and iron carbides.

# X-RAY IMAGING – TOMOGRAPHY

**5D tomographic diffraction imaging (XRD-CT) experiment of a Ni-Pd/CeO<sub>2</sub>-ZrO<sub>2</sub>/Al<sub>2</sub>O<sub>3</sub> catalyst used for methane reforming:** tracking the chemical evolution of many particles across the catalyst bed and relate these changes to the gas environment that the particles experience



Capturing the evolution of the Ni-containing species and gain a more complete insight into the multiple roles of the CeO<sub>2</sub>-ZrO<sub>2</sub> promoters and the reasons behind the partial deactivation of the catalyst during partial oxidation of methane.

# TUNTWIN's Workshop

شكرا

Merci!

Thank you!

¡Gracias!



## CONTACT DETAILS:

**Roberto Boada**

*Associate Professor*

Chemistry Department, Science Faculty

Campus UAB, 08193, Bellaterra

Barcelona, Spain.

Tel.: 0034 93 581 4638

Email: [roberto.boada@uab.cat](mailto:roberto.boada@uab.cat)



Funded by the Horizon 2020 Framework Programme of the European Union under the GA N° 952306

